Geosciences and Engineering, Vol. 12, No. 2 (2024), pp. 93–108.
https://doi.org/10.33030/geosciences.2024.02.008

MITIGATING METAL LOSS IN WASTE PRINTED CIRCUIT BOARDS REVERSE FLOTATION: THE CRITICAL ROLE OF PARTICLE DISPERSION

ALAA ABBADI[1*], LJUDMILLA BOKÁNYI[2]
[1, 2]*Institute of Raw Material Preparation and Environmental Processing, University of Miskolc, Hungary*
[1*]*abbadi.alaa.imad@uni-miskolc.hu*
[2]*ljudmilla.bokanyi@uni-miskolc.hu*
[1]*https://orcid.gov/0009-0003-9533-7078*
[2]*https://orcid.gov/0000-0003-2038-6556*

Abstract: Froth flotation is emerging as a key technique in Waste Printed Circuit Board (WPCB) recycling, but its efficiency is hindered by the spontaneous aggregation of hydrophobic non-metallic particles, which entrap metals and promote foam formation. This study investigates particle aggregation during pulping and evaluates intense agitation as a pretreatment strategy, focusing on the effect of agitation energy on particle dispersion and its direct impact on flotation. Results showed that aggregation decreased with increasing agitation, reaching optimal dispersion with an Aggregation Index (AI) of 6.6% ±2.5% at 1500 rpm; however, higher energy (2000 rpm) led to foam formation and worsened dispersion (AI = 39.8% ±6.3%), with significant metal entrapment. Flotation outcomes correlated directly with dispersion: increasing stirring speed from 500 to 1500 rpm raised underflow metal recovery from 51.71% to 79.34%. These findings establish a quantitative link between agitation energy, dispersion, and flotation performance, providing a practical pathway through optimized intense agitation pretreatment to facilitate pulping, reduce metal losses, and enhance WPCB reverse flotation efficiency.

Keywords: *WPCBs, Flotation, Dispersion, Aggregation*

1. INTRODUCTION

A major bottleneck in the reverse flotation of waste printed circuit boards (WPCBs) is the poor dispersion of particles within the flotation pulp, primarily due to the aggregation of hydrophobic non-metallic particles (Dai et al., 2021; Das et al., 2021; Han et al., 2018; He and Duan, 2017; Vidyadhar and Das, 2013). This aggregation disrupts selective bubble-particle attachment, which is fundamental to flotation efficiency (Sajjad and Otsuki, 2022; Yang et al., 2023). While the impact of interfacial forces on dispersion and flotation performance is well-established in mineral processing, their role in WPCB systems remains insufficiently investigated. This gap limits the optimization of flotation performance, as unresolved particle aggregation directly contributes to metal loss and poor separation efficiency.

Current research has explored various strategies to improve dispersion in WPCB flotation systems, but most remain limited to lab-scale applications with poor

scalability. Pulping methods involving paste formation followed by dilution have been used to overcome particle floating tendencies upon adding to water, yet offer no viable path for industrial application (Ogunniyi, 2009). Ultrasonic treatment shows potential for enhancing dispersion during pulping or aeration stages (Chen et al., 2023; Wang et al., 2021), but its industrial implementation is constrained by high energy demands and operational complexity (Jeldres et al., 2019). More commonly, intense agitation pretreatment has been employed (Burat et al., 2023; Keleş et al., 2024; Zhu, Ni et al., 2020; Zhu, Zhang et al., 2020), drawing from coal flotation studies where it breaks aggregates, cleans surfaces, and improves flotation performance (Yu et al., 2017). However, in the context of WPCBs, the role of agitation energy input during pretreatment remains largely overlooked, despite its known effects on slurry rheology, reagent interaction, and particle aggregation dynamics (Yang et al., 2023).

This study conducts a systematic investigation into dispersion challenges in WPCB flotation by first characterizing particle aggregation during pulping and identifying the mechanisms that contribute to metal loss at flotation initiation. It then assesses intense agitation as a dispersion strategy, using stirring speed as a proxy for energy input during pretreatment. A quantitative approach is introduced to measure the extent of dispersion achieved. Finally, flotation performance is evaluated across agitation intensities to establish the link between energy input, particle dispersion, and metal recovery.

The novelty of this work lies in isolating and quantifying the effect of agitation energy input on particle dispersion and its direct impact on flotation performance in WPCB systems—an area previously overlooked. By clarifying how aggregation dynamics drive metal loss, this study offers a practical framework for controlling dispersion to improve metal recovery and enhance the overall efficiency of WPCB reverse flotation.

2. MATERIALS AND METHODS

2.1. Sample preparation

A feed sample of 30 kg of depopulated WPCBs was obtained from an e-waste facility for this study, comprising mixed-value boards sourced from PCs, servers, switchboards, and various household appliances. The sample predominantly consisted of multilayer and double-sided boards, with a smaller proportion of single-sided types. The preparation of WPCB flotation feed involved a two-stage comminution process followed by mechanical separation *(Figure 1)*.

In the first comminution stage, an axial gap rotary shear with low circumferential speed rotors performed the initial size reduction, cutting WPCB panels to sizes suitable for the hammer shredder's feeding opening. The rotary shear has 10 mm thick discs with a 20 mm front knife depth. The axial and radial gaps were 0.2 mm and 8 mm, respectively. A modified hammer shredder, converted from a mineral crusher, featured a straight anvil, reinforced sieve, and heavier hammers, operating

with an 18 mm screen. The second stage utilized a high-speed impact mill with a tip speed of 80 m/s and a 2 mm internal screen, further reducing particle size.

Mechanical separation of the comminuted material was carried out in three stages. First, a cross belt magnetic separator (350 mm sender belt width, 20–140 mm adjustable gap, 200 × 310 mm magnet dimensions, 0.5 Tesla flux density, 1.1 kW drive motor, 1 m/s max belt speed) removed ferromagnetic particles. Next, an Eriez HDECS eddy current separator, featuring 7 pairs of rare-earth metal magnets, separated non-ferrous metals. For this study, the eddy current separator operated at 1600 rpm drum revolution and 0.5 m/s belt speed. The final stage utilized an Eriez Magnetics electrostatic drum separator, operated at a drum speed of 30 rpm and an applied voltage of 20 kV. The electrode was positioned 50 mm from the drum, and the separation splitter was set at an angle of approximately 80°.

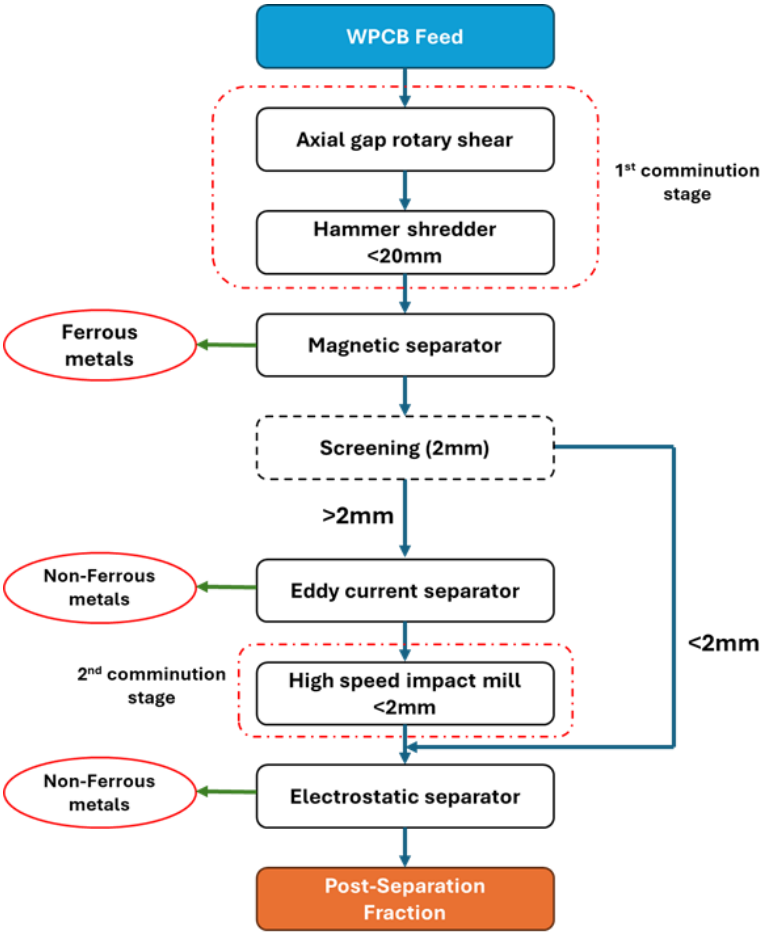

Figure 1

Flowchart of preparation stages for WPCB prior to flotation

2.2. Grinding

Grinding tests were conducted in a laboratory-scale tumbling mill, measuring 19 cm in diameter and 18 cm in length. The experiments used alloy steel balls as the grinding media, with a density of 7.62 g/cm^3. The total mass of the grinding balls was 6.1 kg, achieving a 26.16% fill rate of the mill's volume. A 220 g sample of feed material was used, corresponding to a fractional powder filling of 9.15%. The ball mill operated continuously for 60 minutes. The product was then screened at 0.25 mm, and the fraction below this size was chosen as the feed material for the flotation process.

2.3. Flotation Process

The flotation tests were carried out using a 1L KHD Humboldt Wedag lab mechanical flotation cell. The conditioning strategy tested in this study is illustrated in *Figure 2*. For intense agitation pretreatment, the sample was dispersed in deionized water at 10 wt.% solids and stirred at four different stirring speeds: 500 rpm (1.3 m/s), 1000 rpm (2.6 m/s tip speed), 1500 rpm (3.9 m/s) and 2000 rpm (5.2 m/s). This setup consisted of a four-baffle agitated tank with a four-bladed radial impeller. The 50 mm diameter impeller was positioned 30 mm from the tank bottom. After 15 minutes of stirring, the slurry was transferred to the flotation cell, where the frother was added and conditioned for 2 minutes.

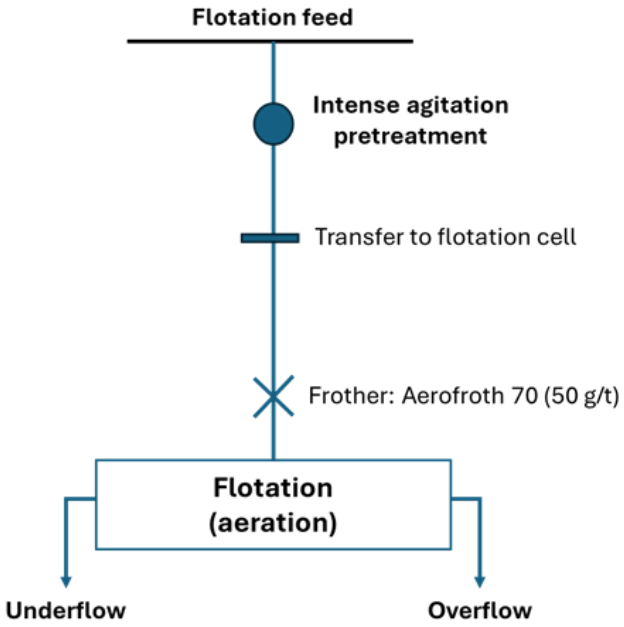

Figure 2
The flowsheets for the flotation experiments

The reagent dosage, impeller speed, and airflow rate were consistent across all flotation experiments, set at 50 g/t frother, 1375 rpm impeller speed, and 2 L/min airflow rate. After each flotation experiment, the overflow and underflow products were collected and dried in an oven for 24 hours at 105 °C. Finally, representative dry samples were prepared for chemical analysis to calculate grades and recovery.

2.4. Characterization

Characterization of WPCP components was conducted using a digital optical microscope (ZEISS Axio Imager). Chemical analyses were carried out at Kisanalitika Ltd., Sajóbábony by ICP-OES method.

To analyze the effect of the conditioning strategy on particle size distribution (PSD), a sample was taken immediately after the agitation step for each conditioning strategy and analyzed by wet sieving. Wet sieving measurements were conducted in triplicate to assess aggregation behavior and the effectiveness of different dispersion methods. To quantify deviations from the dry-basis PSD, the AI was calculated by comparing the PSDs obtained from wet sieving after each conditioning stage to the PSD from dry sieving measurement. The AI, defined by *Equation (1)*, provides a numerical representation of the degree of aggregation

$$\mathrm{AI} = \frac{1}{n}\sum_{i=1}^{n}\left|\frac{\mathrm{wet}_i - \mathrm{dry}_i}{\mathrm{dry}_i}\right| \times 100 \quad (1)$$

where n is the number of size fractions, wet i is the percentage distribution for a given conditioning strategy based on wet sieving, and dry i is the percentage distribution from dry sieving. Lower AI values indicate better performance, signifying a closer match to the dry distribution and, consequently, better dispersion of WPCB particles in water.

3. RESULTS AND DISCUSSION

3.1. Flotation feed characterization

The chemical analysis of the WPCB flotation feed, summarized in Table 1, reveals the concentration of valuable metals.

Table 1

Metal content of WPCB flotation feed

Element	Cu	Fe	Ni	Pb	Zn	Ag	Au
Content (wt.%)	2.3	0.53	0.24	0.10	0.43	0.02	0.006

Figure 3 shows the yield of size fractions and the corresponding metal distribution. The finest fraction (<0.075 mm) had the highest yield (47.6%), consistent with the breakage of brittle polymers and ceramics (Nekouei et al., 2018).

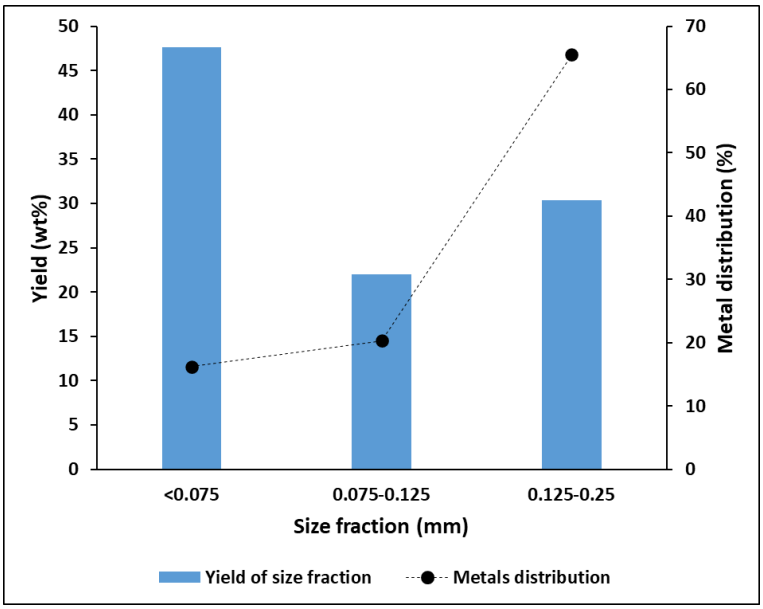

Figure 3
Yield and metals distribution (%) with various size fractions below 0.25 mm used for flotation

In contrast, metal distribution was concentrated in coarser fractions, with 65% of metals found in the 0.125–0.25 mm range, dropping to 16% in the <0.075 mm product. This confirms that metallic components preferentially report to larger size fractions due to their elastic-plastic breakage behavior under mechanical stress, which limits their fragmentation during grinding.

3.2. Aggregation

The initial observation indicates that despite the true density of the WPCB flotation feed being 1.7 g/cm³, the introduction of the WPCB sample into the water for flotation pulp preparation was hindered by the aggregation phenomenon. This resulted in the formation of both completely dry aggregates and partially wetted surface aggregates where the inner particles remained dry. Consequently, their low bulk density caused them to float on the pulp surface *(Figure 4)*.

The immediate formation of dry and partially wetted aggregates upon adding WPCB sample to water can be primarily attributed to the hydrophobic nature of the non-metallic components of WPCBs. Zeta potential measurements as a function of pH *(Figure 5)* revealed that the non-metal particles have a negatively charged surface in a neutral solution, resulting in repulsive forces between them. This rules out electrostatic attraction as a mechanism for non-metal aggregation. Therefore, the predominant forces causing aggregation are the hydrophobic attraction forces (Han et al., 2018). The hydrophobic attraction between particles immersed in water is an effective interaction that arises from the high free energy of cohesion among

surrounding water molecules – particularly the hydrogen-bonding network. When nonpolar surfaces approach each other, structured water at the interface is displaced, reducing the system's free energy and resulting in an apparent attractive force (Van Oss, 2003).

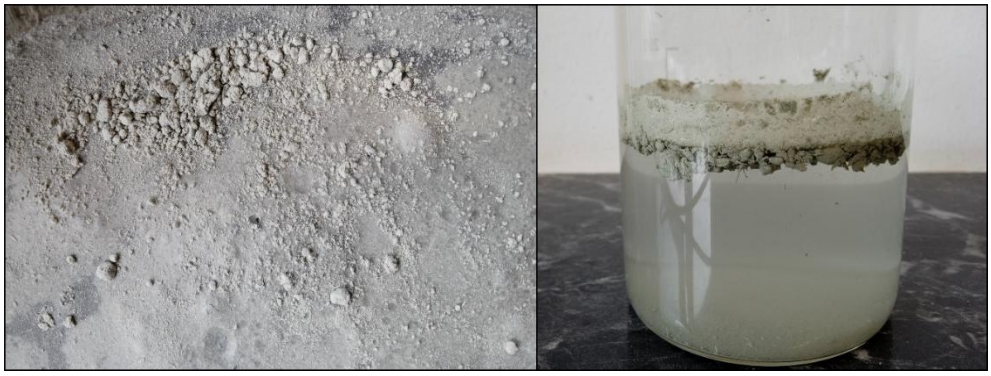

Figure 4
Immediate formation of dry and wet aggregates after adding dry powder of WPCBs to water

The hydrophobicity of WPCB non-metals stems from the organic resins used in WPCB manufacturing (Nie et al., 2023). During production, fiberglass is impregnated with these resins, which are difficult to remove completely by comminution (Kumar et al., 2015). Consequently, the residual resin influences the surface characteristics of both the resin particles and the impregnated fiberglass (Kumar et al., 2020). The WPCB non-polar hydrophobic surfaces tend to minimize their contact area with water, leading to an induced attractive force that causes aggregation.

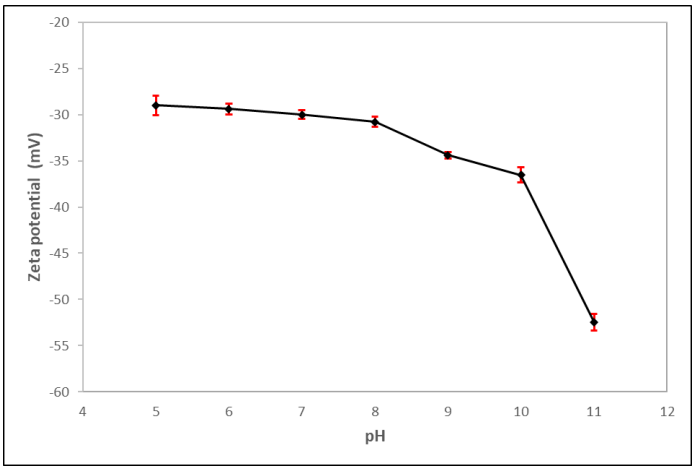

Figure 5
Zeta potential of WPCB non-metal in different pH aqueous solutions

The formation of non-metal aggregates, where they can unselectively entrap metallic particles, poses a significant challenge in the flotation process, as inadequate dispersion may allow these aggregates to persist throughout the conditioning stage and remain within the pulp. This persistence increases the likelihood of their transfer to the froth zone upon flotation initiation.

3.3. Assessment of conditioning

To analyze the aggregation behavior of the WPCB flotation feed and evaluate the effect of intense agitation on dispersion, dry and wet particle size distributions were determined using sieve analysis. While sieve analysis presents limitations due to the energy applied, which may disrupt pre-existing aggregates, it enables the evaluation of the entire batch of samples. Several assumptions underpin this approach: dry sieving approximates a dispersed state due to the absence of water-mediated interactions; particle aggregation manifests as an upward shift in size distribution to coarser fractions (>0.125 mm); and in the absence of aggregation, wet sieving results should closely align with dry sieving. Therefore, deviations from dry sieving baselines are interpreted as aggregation indicators.

Figure 6 presents the size distribution of the suspension under different stirring speeds following the agitation stage. The deviations observed between the dry and wet size distributions highlight the influence of stirring speed as a proxy for energy input in the system.

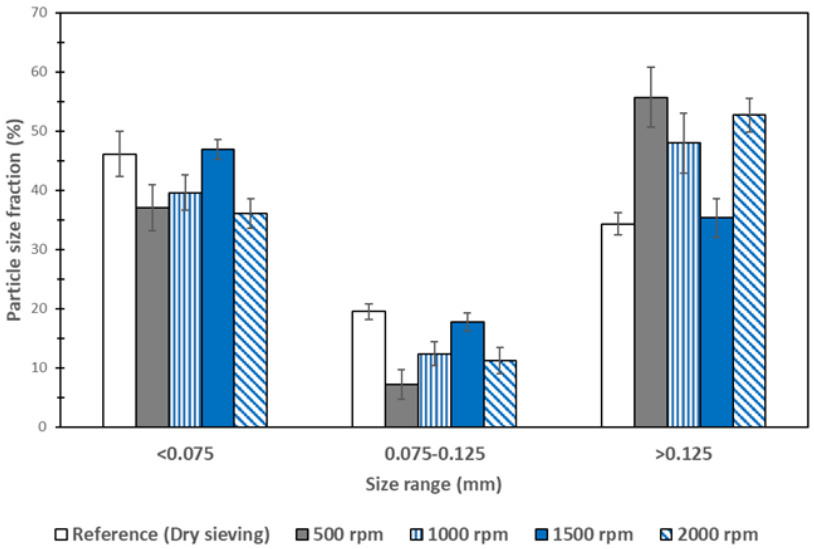

Figure 6
Particle size distribution of WPCB particles after intense agitation at different stirring speeds

Following intense agitation at 500 rpm, a significant shift in particle distribution is observed. The coarse fraction (>0.125 mm) increases markedly to 55.7% ±5.1%, while the intermediate (0.075–0.125 mm) and fine (<0.075 mm) fractions decrease to 7.2% ±2.5% and 37.1% ±3.9%, respectively.

This contrasts with the dry sieving reference, where these fractions were 34.3% ±3.8%, 19.5% ±2.0%, and 46.2% ±1.8%, respectively. The observed increase in coarse fraction and reduction in fine fractions indicate poor dispersion and aggregation within the pulp.

While aggregation persists across all stirring speeds, its extent diminishes with increasing energy input up to an optimal point. This trend is quantified by AI as depicted in *Figure 7*. At 1500 rpm, the lowest AI value of 6.6% ±2.5% is achieved, indicating the most effective dispersion. In contrast, 500 and 1000 rpm exhibit severe aggregation, with AI values of 48.5% ±10.4% and 30.4% ±10.7%, respectively. The substantial difference in AI values underscores the critical role of energy input in destabilizing hydrophobic aggregates, as supported by literature on shear flocculation in mineral processing (Shen and Zhang, 2022).

Higher stirring speeds generate intense shear that disrupts metastable hydrophobic aggregates. The applied mechanical energy overcomes the cohesive interfacial forces that exclude water from particle contact zones. This action forces water infiltration and breaks air pockets within the aggregates, reducing hydrophobic contact and enabling more uniform dispersion throughout the pulp. However, beyond the optimal stirring speed, excessive energy input may not yield further improvements and can even degrade dispersion. This is evident at 2000 rpm, where dispersion deteriorates despite the high energy input.

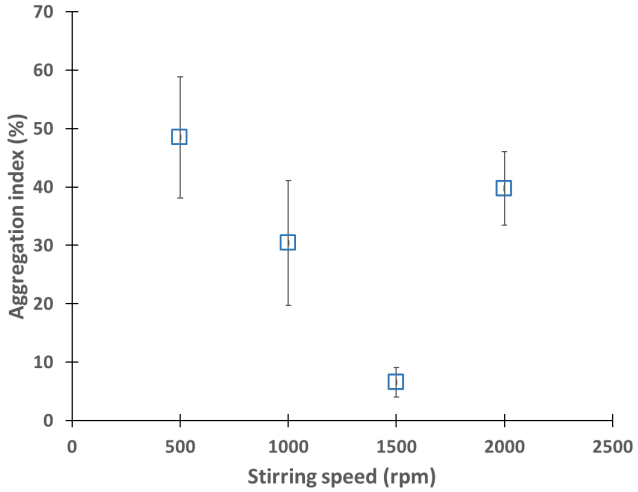

Figure 7

Effect of stirring speed on aggregation index following intense agitation pretreatment

Notably, while 500 and 1000 rpm did not achieve effective dispersion, they also avoided foam layer formation, a phenomenon discussed in detail next. In contrast, the 1500 rpm stirring speed not only achieved the best dispersion but also minimized foam formation, contributing to the slight deviation from the reference PSD. This suggests that 1500 rpm operates within the optimal energy range, providing sufficient energy to disrupt hydrophobic interactions without inducing adverse effects.

At a stirring speed of 2000 rpm, the WPCB suspension exhibited higher aggregation and poorer dispersion compared to 1500 rpm, despite the increased energy input. This is reflected in the AI, which reached 39.8%± 6.3%, indicating a significant reversal in dispersion efficiency. This unexpected trend is primarily attributed to the formation of a stable foam layer at the pulp-air interface *(Figure 8)*, where WPCB non-metallic particles adhere to air bubbles introduced through increased turbulence. A similar phenomenon was reported with flaky graphite particle systems (Yangshuai et al., 2017).

Figure 8

Stable foam layer at the pulp-air interface formed solely by high-speed agitation at 2000 rpm (no aeration or frother addition)

The formation of this layer at the pulp-air interface results from a complex interplay between WPCB particle characteristics and hydrodynamic conditions. Previous research has established that WPCB pulp can generate a stable froth phase upon aeration in surfactant-free conditions, through particle-mediated mechanisms (Ogunniyi and Vermaak, 2009). While conventional two-phase froth systems typically require reduced surface tension, three-phase systems can achieve stabilization through fine particles without necessitating such reductions in surface tension.

The hydrodynamic conditions generated at 2000 rpm play a pivotal role in this phenomenon. Increased turbulence at this high stirring speed introduces a significant quantity of air into the system, while the abundance of fine particles provides a large surface area for stabilizing bubble walls. This dynamic stabilization closely

resembles froth formation, where fine particle flocculation strengthens bubble interstices, maintaining foam integrity even without surfactants.

The foam layer was collected and subjected to PSD, SEM, and chemical analyses. The PSD results confirmed that 86% of the particles in the foam were finer than 0.075 mm, while a combined 14% were coarser. This finding aligns with the proposed mechanism, where fine particles contribute to stabilization while coarser particles may be entrapped as aggregates or individual particles. More critically, microscopic images provided direct evidence of metallic particle presence within the foam layer, as shown in *Figure 9*.

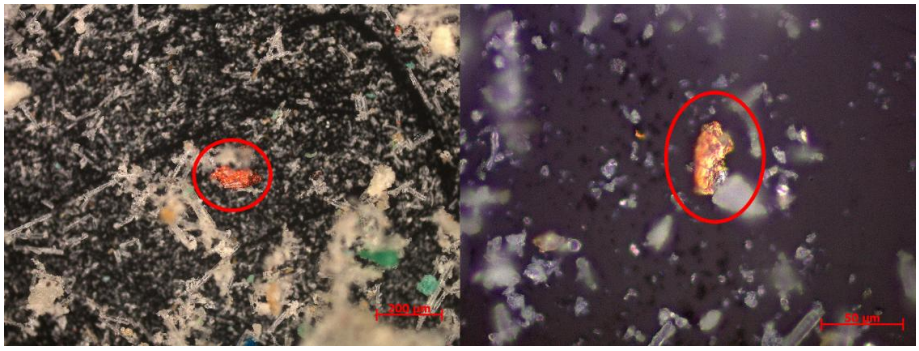

Figure 9

Microscopic evidence of metallic particle entrapment within the foam layer

Chemical analysis further quantified the extent of metal entrapment in the foam, revealing notable metal concentrations: 5.7 g/kg copper, 2.2 g/kg zinc, 0.5 g/kg lead, 1 g/kg nickel, 10 g/kg iron, 212 mg/kg silver, and 22.6 mg/kg gold. These findings indicate that the foam layer can serve as a significant pathway for unintended metal losses during flotation. The persistence of this foam layer at 2000 rpm suggests that beyond an optimal stirring speed, further energy input not only fails to improve dispersion but also exacerbates metal losses by promoting the entrapment of metals within stabilized foam structures.

3.4. Flotation Results

As shown in *Figure 10*, variations in stirring speed significantly influenced both the overflow yield and the underflow metal recovery. Increasing the stirring speed from 500 to 1500 rpm resulted in a decline in overflow yield from 81.62% to 75.91%, while underflow metal recovery improved from 51.71% to 79.34%. These trends can be directly linked to the extent of aggregation formed during the intense agitation pretreatment.

A clear relationship emerges between the degree of aggregation and flotation performance. Higher aggregation levels, such as those observed at 500 rpm, contributed to increased overflow yield, while the lowest aggregation level at 1500 rpm corresponded to the lowest overflow yield. The aggregation increases the apparent particle size with low bulk density, as non-metallic hydrophobic clusters

entrap air pockets, forming larger, low-density structures. These aggregates exhibited enhanced buoyancy, persisting at the pulp-air interface and easily reporting to the overflow upon aeration.

Furthermore, aggregation also impacted underflow metal recovery. The unselective nature of these aggregates, which entrap metallic particles, explains the trend in underflow metal recovery. As dispersion improves with increased stirring speed, metal entrapment within aggregates diminishes, leading to a more selective flotation process and higher metal recovery in the underflow. A similar effect of WPCB particle aggregation on flotation selectivity has been reported, where optimal dispersion conditions yielded the highest metal recovery (Chen et al., 2023). The findings support the relevance of the aggregation index as a comparative tool, with its trend closely reflecting the observed flotation performance.

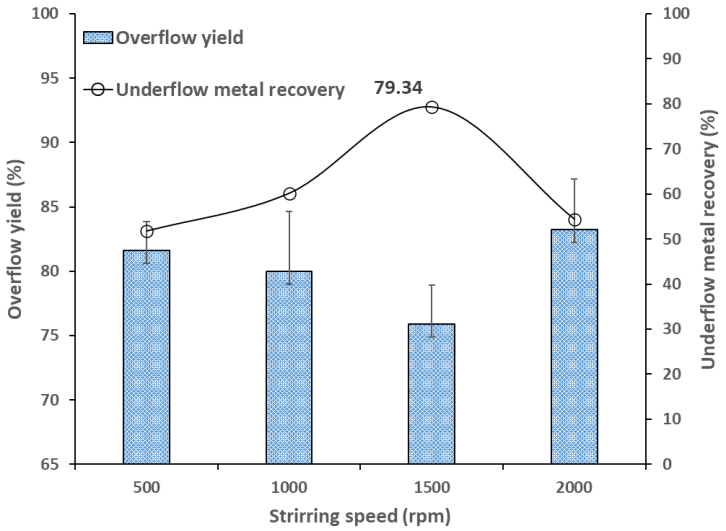

Figure 10
Effect of stirring speed during intense agitation pretreatment on flotation performance

The flotation behavior following intense agitation at 2000 rpm deviates from the previously observed trends. Here, the dominant factor is not aggregation but rather the formation of a stable foam layer at the pulp-air interface, a phenomenon unique to the highest turbulence condition. Upon aeration, this foam layer reports directly to the overflow, significantly increasing the overflow yield to 83.25%. Additionally, the foam layer's ability to entrap metallic particles exacerbates metal losses, as it creates a physical barrier that prevents metals from settling into the underflow. Consequently, flotation after 2000 rpm agitation pretreatment results in low underflow metal recovery at 54.36%.

4. CONCLUSIONS

The inherent hydrophobicity of WPCB non-metallic particles resulting from residual organic resins used in manufacturing, drives complex behaviors in aqueous systems. These non-polar surfaces minimize contact with water, leading to hydrophobic attraction forces that manifest in two key pathways detrimental to flotation performance. First, spontaneous aggregation during pulp preparation forms buoyant clusters that entrap metallic particles and hinder selective separation. Second, fine hydrophobic particles stabilize air bubbles introduced by turbulence, generating a persistent, metal-laden foam layer at the pulp-air interface.

Intense agitation was investigated as a pretreatment strategy to enhance dispersion, with stirring speed being a critical factor. The application of intense agitation effectively and irreversibly broke up aggregates, releasing entrapped metals and significantly improving particle dispersion. This was consistently observed as enhanced metal recovery in reverse flotation, particularly following the optimized stirring speed. However, when the stirring speed exceeded this optimal range, excessive turbulence promoted the foam formation at the pulp-air interface. This foam layer, stabilized by fine hydrophobic particles, acted as a secondary site for metal entrapment and contributed to increased losses to the overflow.

Future work will focus on the distinct flotation behaviors of individual metals, which are obscured when recovery is assessed in bulk. Despite optimized pretreatment, significant and variable losses of specific metals to the overflow were observed under uniform flotation conditions. This highlights the need to shift toward metal-specific analysis, considering how factors such as liberation, morphology, and composition influence recovery. Such an approach is essential for developing targeted strategies that maximize economic value rather than bulk recovery.

ACKNOWLEDGMENTS

The authors would like to express their gratitude to István Balika from Metalex 2001 Kft. for providing the waste printed circuit board samples used in this study. We also thank Kisanalitika Ltd., Sajóbábony for conducting the chemical analysis of the flotation samples.

REFERENCES

Burat, F., Dinç, N. İ., Dursun, H. N., Ulusoy, U. (2023). The Role of Particle Size and Shape on the Recovery of Copper from Different Electrical and Electronic Equipment Waste. *Minerals*, 13 (7). https://doi.org/10.3390/min13070847

Chen, L., He, J., Zhu, L., Yao, Q., Sun, Y., Guo, C., Chen, H., Yang, B. (2023). Efficient recovery of valuable metals from waste printed circuit boards via ultrasound-enhanced flotation. *Process Safety and Environmental Protection*, 169 (September 2022), pp. 869–878. https://doi.org/10.1016/j.psep.2022.11.046

Dai, G., Han, J., Duan, C., Tang, L., Peng, Y., Chen, Y., Jiang, H., Zhu, Z. (2021). Enhanced flotation efficiency of metal from waste printed circuit boards modified by alkaline immersion. *Waste Management*, 120, pp. 795–804. https://doi.org/10.1016/j.wasman.2020.11.002

Das, S. K., Ellamparuthy, G., Kundu, T., Ghosh, M. K., Angadi, S. I. (2021). Critical analysis of metallic and non-metallic fractions in the flotation of waste printed circuit boards. *Powder Technology*, 389, pp. 450–459. https://doi.org/10.1016/j.powtec.2021.05.061

Gouvêa Junior, J. T., Chipakwe, V., de Salles Leal Filho, L., Chehreh Chelgani, S. (2023). Biodegradable ether amines for reverse cationic flotation separation of ultrafine quartz from magnetite. *Scientific Reports*, 13 (1), pp. 1–16. https://doi.org/10.1038/s41598-023-47807-0

Han, J., Duan, C., Li, G., Huang, L., Chai, X., Wang, D. (2018). The influence of waste printed circuit boards characteristics and nonmetal surface energy regulation on flotation. *Waste Management*, 80, pp. 81–88. https://doi.org/10.1016/j.wasman.2018.09.002

He, J., Duan, C. (2017). Recovery of metallic concentrations from waste printed circuit boards via reverse floatation. *Waste Management*, 60, pp. 618–628. https://doi.org/10.1016/j.wasman.2016.11.019

Jeldres, R. I., Uribe, L., Cisternas, L. A., Gutierrez, L., Leiva, W. H., Valenzuela, J. (2019). The effect of clay minerals on the process of flotation of copper ores – A critical review. *Applied Clay Science*, 170 (January), pp. 57–69. https://doi.org/10.1016/j.clay.2019.01.013

Kar, U., Nili, S., Mends, E., Vahidi, E., Chu, P. (2025). A review and environmental impact analysis on the current state of froth flotation on recycling of e-wastes. *Resources, Conservation and Recycling*, 212 (June 2024). https://doi.org/10.1016/j.resconrec.2024.107967

Keleş, B., İlkyaz Dinç, N., Nur Dursun, H., Burat, F., Ulusoy, U. (2024). The effect of particle geometry (size & shape) on the recovery of gold and copper metallic particles from end-of-life random access memory cards by flotation. *Waste Management*, 179 (February), pp. 66–76. https://doi.org/10.1016/j.wasman.2024.03.008

Kumar, A., Holuszko, M. E., Janke, T. 2020. Examining the surface properties of waste printed circuit boards rejects using inverse gas chromatography. *Resources, Conservation and Recycling*, 163 (August), 105093. https://doi.org/10.1016/j.resconrec.2020.105093

Kumar, V., chun Lee, J., Jeong, J., Jha, M. K., su Kim, B., Singh, R. (2015). Recycling of printed circuit boards (PCBs) to generate enriched rare metal concentrate. *Journal of Industrial and Engineering Chemistry*, 21, pp. 805–813. https://doi.org/10.1016/j.jiec.2014.04.016

Nekouei, R. K., Pahlevani, F., Rajarao, R., Golmohammadzadeh, R., Sahajwalla, V. (2018). Two-step pre-processing enrichment of waste printed circuit boards: Mechanical milling and physical separation. *Journal of Cleaner Production*, 184, pp. 1113–1124. https://doi.org/10.1016/j.jclepro.2018.02.250

Nie, C. chen, Jiang, S. qi, Li, X. guang, Lyu, X. jun, Zhang, Y. qing, Zhu, X. nan. (2023). Surface characteristic driven in waste printed circuit boards flotation: Floatability mechanism of resin and glass fiber in non-metallic component. *Process Safety and Environmental Protection*, 178 (August), pp. 360–369. https://doi.org/10.1016/j.psep.2023.08.024

Ogunniyi, I. O. (2009). *Investigation into Froth Flotation for The Beneficiation of Printed Circuit Board Comminution Fines* (Issue September). University of Pretoria.

Ogunniyi, I. O., Vermaak, M. K. G. (2009). Investigation of froth flotation for beneficiation of printed circuit board comminution fines. *Minerals Engineering*, 22 (4), pp. 378–385. https://doi.org/10.1016/j.mineng.2008.10.007

Otsuki, A., Bryant, G. (2015). Characterization of the interactions within fine particle mixtures in highly concentrated suspensions for advanced particle processing. *Advances in Colloid and Interface Science*, 226, pp. 37–43. https://doi.org/10.1016/j.cis.2015.07.005

Sajjad, M., Otsuki, A. (2022). Correlation between Flotation and Rheology of Fine Particle Suspensions. *Metals*, 12 (2), pp. 1–31. https://doi.org/10.3390/met12020270

Shen, Z., Zhang, Q. (2022). Hydrophobic agglomeration behavior of rhodochrosite fines Co-induced by oleic acid and shearing. *Separation and Purification Technology*, 282 (PB), 120115. https://doi.org/10.1016/j.seppur.2021.120115

Van Oss, C. J. (2003). Long-range and short-range mechanisms of hydrophobic attraction and hydrophilic repulsion in specific and aspecific interactions. *Journal of Molecular Recognition*, 16 (4), pp. 177–190. https://doi.org/10.1002/jmr.618

Vidyadhar, A., Das, A. (2013). Enrichment implication of froth flotation kinetics in the separation and recovery of metal values from printed circuit boards. *Separation and Purification Technology*, 118, pp. 305–312. https://doi.org/10.1016/j.seppur.2013.07.027

Wang, C., Sun, R., Xing, B. (2021). Copper recovery from waste printed circuit boards by the flotation-leaching process optimized using response surface methodology. *Journal of the Air and Waste Management Association*, 71 (12), pp. 1483–1491. https://doi.org/10.1080/10962247.2021.1874568

Yang, S., Wu, Y., Chai, W., Cao, Y. (2023). Effect of energy input on surface properties and dispersion of diaspore and kaolinite in flotation process. *Chemical Engineering and Processing – Process Intensification*, 192 (June), 109518. https://doi.org/10.1016/j.cep.2023.109518

Yangshuai, Q., Yongfu, Y., Lingyan, Z., Weijun, P., Yupeng, Q. (2017). Dispersion and agglomeration mechanism of flaky graphite particles in aqueous solution. *Journal of Dispersion Science and Technology*, 38 (6), pp. 796–800. https://doi.org/10.1080/01932691.2016.1198703

Yao, Y., Bai, Q., He, J., Zhu, L., Zhou, K., Zhao, Y. (2020). Reverse flotation efficiency and mechanism of various collectors for recycling waste printed circuit boards. *Waste Management*, 103, pp. 218–227. https://doi.org/10.1016/j.wasman.2019.12.030

Yu, Y., Cheng, G., Ma, L., Huang, G., Wu, L., Xu, H. (2017). Effect of agitation on the interaction of coal and kaolinite in flotation. *Powder Technology*, 313, pp. 122–128. https://doi.org/10.1016/j.powtec.2017.03.002

Zhu, X. nan, Ni, Y., Wang, D. zhang, Zhang, T., Qu, S. juan, Qiao, F. ming, Ren, Y. guang, Nie, C. chen, Lyu, X. jun, Qiu, J., Li, L. (2020). Effect of dissociation size on flotation behavior of waste printed circuit boards. *Journal of Cleaner Production*, 265, 121840. https://doi.org/10.1016/j.jclepro.2020.121840

Zhu, X. nan, Zhang, L. ye, Dong, S. ling, Kou, W. jia, Nie, C. chen, Lyu, X. jun, Qiu, J., Li, L., Liu, Z. xue, Wu, P. 2020. Mechanical activation to enhance the natural floatability of waste printed circuit boards. *Waste Management*, 109, pp. 222–230. https://doi.org/10.1016/j.wasman.2020.05.008